ORIGINAL RESEARCH

Ultrahigh molecular weight polyethylene fiber/boron nitride composites with high neutron shielding efficiency and mechanical performance

Wei Zhang[1] · Yao Feng[1] · Jalal T. Althakafy[2] · Yi Liu[1] · Hala M. Abo-Dief[3] · Mina Huang[4] · Liangchun Zhou[1] ·
Fengmei Su[1] · Chuntai Liu[1] · Changyu Shen[1]

Abstract

Neutron shielding material with high shielding efficiency, small density, and flexibility is urgently needed in nuclear plants, aerospace, and healthcare field. In this study, neutron shielding composite of ultrahigh molecular weight polyethylene fiber (UPEF)/boron nitride (BN)/polyurethane (PU) is fabricated by spraying BN/PU dispersion on UPEF, where UPEF and BN are used to slow and absorb the neutrons, respectively, and PU was used as adhesive matrix, due to that polyethylene (PE) with high content of hydrogen can effectively slow the high-energy neutrons to thermal neutrons through multiple collisions with hydrogen atoms while boron has large capture cross-section for thermal neutrons. The result shows that the neutron transmission factor (I/I_0) of the 3.2-mm-thick UPEF/BN/PU composite decreases to 0.28% at a BN content of 20 wt%. In addition, the composite shows excellent mechanical performance with tensile stress of 550–750 MPa. The UPEF/BN/PU composite is proved effective in neutrons shielding, making it excellent candidate in neutron radiation-related field, both as functional and structural material.

✉ Fengmei Su
 fmsu@zzu.edu.cn

✉ Chuntai Liu
 1005613221@qq.com

 Jalal T. Althakafy
 jtthakafy@uqu.edu.sa

 Hala M. Abo-Dief
 h.abodeif@tu.edu.sa

 Mina Huang
 1005613221@qq.com

[1] National Engineering Research Center for Advanced Polymer Processing Technology, The Key Laboratory of Material Processing and Mold, Ministry of Education, Zhengzhou University, Zhengzhou 450002, People's Republic of China

[2] Chemistry Department, Faculty of Applied Science, Umm Al-Qura University, Makkah, Saudi Arabia

[3] Department of Chemistry, College of Science, Taif University, P.O. Box 11099, Taif 21944, Saudi Arabia

[4] College of Materials Science and Engineering, Taiyuan University of Science and Technology, Taiyuan 030024, People's Republic of China

1 Introduction

The unwanted neutron radiation is frequently encountered in nuclear plants, aerospace, and healthcare-related field. Neutron radiation is a type of ionizing radiation comprising uncharged particles; therefore, it passes through the electron cloud more efficiently than charged particles and interacts directly with the nucleus of the atom and emits harmful radiation, simultaneously [1–6]. Long-term exposure to neutrons will cause severe damage to the nucleus of human tissues, resulting in diseases, like cancer, cardiovascular diseases, leukemia, cataracts, and neurological diseases [7–9]. The most common materials used for the attenuation of neutron radiation are concrete and metal materials like aluminum because of their low cost and user-friendliness [10, 11]. However, their high density and large volume severely restrict their application in aerospace area, particularly as wearable protection devices, which will limit the movement of astronauts' limbs and lead to their movement burden [12]. Most importantly, numerous investigations have demonstrated that the collision of neutrons with metal materials will produce abundant heavy isotope impurities

and target fragments, which are sources of secondary radiation [13–15]. Therefore, these traditional shielding materials cannot meet the key requirements for application in specific applications such as deep space missions and portable devices, so new efficient neutron shielding materials with properties of flexibility, low density, and low secondary emissions are in urgent needed [16].

The shielding of neutrons includes the scattering and deceleration of fast neutrons and the absorption of thermal neutrons [17–19]. According to the law of conservation of momentum and energy, when the mass of a neutron is equal to that of the target nucleus, the energy of the neutrons can be transferred more effectively through neutron scattering of the target nucleus [20, 21]. In this case, hydrogen with one neutron in its nucleus may have the highest efficiency to slow down the neutrons [19]. Zeitlin et al. have demonstrated that hydrogen is by far the most effective material in slowing high-energy neutrons [22]. Polyethylene (PE), which only comprises atoms with low atomic number (carbon and hydrogen) and contains the highest content of hydrogen among solid state materials, is frequently used as a polymer matrix for neutron shielding [23, 24]. A special class of PE materials, ultrahigh molecular weight polyethylene fiber (UPEF) produced via gel-spinning technology, has extraordinary mechanical properties (high specific modulus and strength, high cut, and abrasion tolerance), low density (0.97 g/cm^3), excellent chemical resistance, low dielectric constant, and moisture absorption, which makes UPEF a candidate spacesuit material [25–29]. Zhong et al. fabricated UPEF/nanoepoxy composites that showed high radiation shielding effectiveness [30]. In addition, boron-containing fillers are excellent for thermal neutron absorption because boron can absorb neutrons with a wide energy range. Boron has a significantly high neutron capture cross-section for thermal neutrons of approximately 3840 barns (10^{-24} cm^2) [31, 32]. The fabrication of composite is a very convenient way to endow materials with more functions [33, 34]. Moreover, the main products of boron and neutron reactions (alpha particles) show a large mass, short range, and weak penetration ability, which can be shielded easily [35]. Boron-containing materials such as boron nitride (BN) and boron carbide (B$_4$C) have been added to polymers, such as PE, polypropylene (PP), and epoxy to fabricate radiation-shielding composites [36, 37]. Shang et al. prepared multilayer PE/BN composite films with alternating high-density polyethylene (HDPE)/BN layers and low-density polyethylene (LDPE) layers for high-efficiency neutron shielding [38]. PE/BN composite achieves high neutron shielding efficiency as it combines the deceleration effect of PE and the absorption effect of BN on neutrons.

Based on the above analysis, composites with UPEF and BN may be a good strategy for neutron radiation shielding. In this work, an UPEF/BN/PU composite was fabricated, where the continuous UPEF was used as neutron moderator and mechanical reinforcement, BN as neutron absorber fillers. In addition, polyurethane (PU) was used as polymer matrix [39–43]. Considering that the dispersion of fillers in the matrix is crucial for the neutron shielding materials, as the improvement of the dispersion of the fillers in the matrix will lead to increase of the probability of collision between the fillers and neutrons; thereby, the homogenously dispersion of BN in the composites is necessary [44–47]. Because PE and BN showed poor interfacial adhesion, the modification of BN is an effective method to improve its dispersion [48–55]. Thus, we firstly modified the BN with tannic acid (TA) to prepare BN/PU dispersion, and then sprayed BN/PE dispersion on UPEF fabrics. As a result, the neutron shielding measurement on the composite with thickness of 3.2 mm and BN content of 20 wt% showed that the neutron transmission factor (I/I_0) decreased to 0.28%. Notably, the composite shows outstanding high tensile stress of 550–750 MPa, indicating that the composite can be used as structural material, which demonstrates impressive potential in applications, such as deep-space aerospace, healthcare, nuclear reactors, and other related fields.

2 Experimental process

2.1 Material

BN platelets with sizes of 1 μm were obtained from Shanghai Naiou Nanotechnology Co., Ltd. Solid TA (C$_{76}$H$_{52}$O$_{46}$, 98%, 2.12 g/cm^3) and tris(hydroxymethyl) amino-methane (Tris) were purchased from Shanghai McLean Biochemical Technology Co., Ltd., Shanghai, China. The UPEF (Dyneema 75*), with density of 0.97 g/cm^3, was obtained from Royal DSM Co., Ltd. The tensile strength and elongation were in ranges of 3.3–3.9 GPa and 3–4%, respectively. Waterborne PU solution (AH-1650F) was obtained from Anhui Anda Huatai New Material Co., Ltd.

2.2 Modification of BN

As shown in Fig. 1, original BN powder (5.0 g) was dispersed in deionized water (500 mL) with ultrasound for 2 h and stirred for 2 h at room temperature. Thereafter, tris (1.5 g) was mixed with the aforementioned BN dispersion with ultrasound for 0.5 h and stirred for 2 h at room temperature. Then, TA (1.5 g) was added and stirred at room temperature for 12 h. Afterwards, the solution was washed with deionized water until the pH of the solution was close to 7. Finally, the sample was dyed in an oven at 60 °C for 24 h to obtain the modified BN, which is denoted hereafter as m-BN.

Fig. 1 Schematic illustration of the fabrication of UPEF/BN/PU
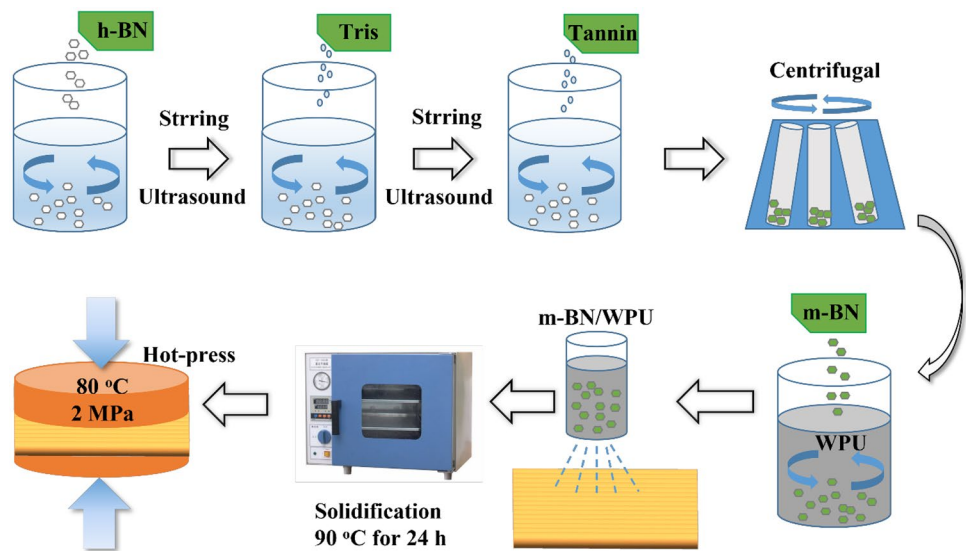
2.3 Preparation of UPEF/BN/PU composite

BN/PU dispersion was prepared by adding 0.2, 0.4, 0.9, 1.6, and 2.5 g m-BN to PU solution (8.0 g). The mass fraction of m-BN in the total m-BN and dried PU was 5%, 10%, 20%, 30%, and 40%, respectively. As shown in Fig. 1, then the BN/PU dispersion was sprayed on the UPEF fabrics (2.7 g). Finally, the samples were dried in an oven at 60 °C for 12 h and hot-pressed at 80 °C under a pressure of 2 MPa for 5 min. The obtained samples were labeled as UPEF/BN/PU-x, where x represents the weight fraction of BN in BN/PU, which are UPEF/BN/PU-5, UPEF/BN/PU-10, UPEF/BN/PU-20, UPEF/BN/PU-30, and UPEF/BN/PU-40, respectively.

2.4 Characterization

Fourier transform infrared (FTIR) spectra were recorded using an FTIR spectrometer (Nicolet iS50) in the attenuated total reflection (ATR) mode. The morphologies were investigated by scanning electron microscopy (SEM, JEOLJSM-7500F) under an acceleration voltage of 10 kV. Thermogravimetric analysis (TGA Netzsch STA 209F3) was conducted to analyze the weight fraction of BN in the composite at a heating rate of 20 °C min^{-1} under air flow. Neutron shielding measurements were performed at China Mianyang Research Reactor (CMRR) [56, 57]. The neutron wavelength of SANS was 0.53 nm, and the sample to detector distance was 10.45 m. The samples for the neutron shielding measurements were cut into squares of 30×30 mm.

Wide angle X-ray diffraction (WAXD) and small angle X-ray scattering (SAXS) measurements were performed with a Bruker D8 Discovery X-ray device with a Cu Kα

X-ray source. The X-ray wavelength was 0.154 nm. For WAXD measurement, the exposure time and sample to detector distance were 60 s and 84.99 mm, respectively. The WAXD patterns were captured by a vantec-500 two-dimensional (2D) detector. For SAXS measurement, the exposure time and the sample to detector distance were 90 s and 1085 mm, respectively, and the SAXS patterns were recorded with a vantec-2000 2D detector. Fit2D software was used to analyze the WAXD and SAXS patterns to obtain one-dimensional (1D) curves and azimuthal angle distribution plots.

Mechanical testing was performed on an electromechanical universal testing machine (Shenzhen Labsans Testing Machine Co., ltd) at a cross head speed of 10 mm/min at room temperature. The size of specimens for the tensile property's measurement was $200 \times 20 \times 0.8$ mm.

3 Results and discussion

3.1 Characterization of m-BN

In order to prepare homogenously BN/PU dispersion, BN was modified with TA to improve its dispersity in aqueous PU solution. As shown in Fig. 2a, TA contains a large amount of catechol and pyrogallol, which can be adsorbed on the surface of BN sheets through π–π interactions. FTIR spectra measurement was carried out to see whether the modification of BN was successful or not. Figure 2b shows the FTIR spectra of BN prior to and after modification; these two characteristic absorption peaks at approximately 1382 cm^{-1} and 809 cm^{-1} are attributed to the stretching vibration of the B–N band and the bending vibration of the B-N-B band, respectively. Notably, the FTIR spectrum of
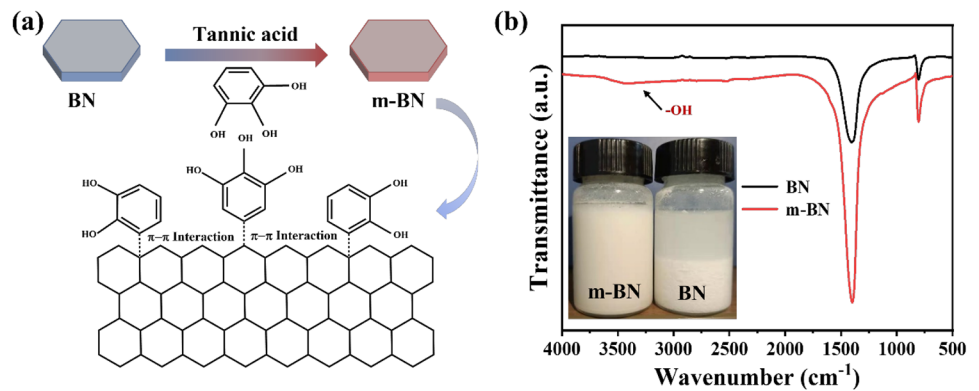
m-BN shows a peak at approximately 3421 cm^{-1}, indicated by the black arrow, which corresponds to the stretching vibration of –OH. The appearance of this peak indicates the successful grafting of TA on the surface of BN. The inset of Fig. 2b shows the image of 10 mg/mL m-BN and BN dispersions in deionized water after the m-BN and BN dispersions were left 24 h. Compared with BN, m-BN was evenly dispersed in deionized water without stratification. The well dispersion of m-BN in water will benefit the preparation of uniform and stable BN/PU dispersion.

3.2 Morphology and structure of UPEF/BN/PU composites

The morphologies and microstructures of the BN, UPEF, and UPEF/BN/PU composites were characterized by SEM, as shown in Fig. 3. The lateral size and thickness of BN are about 1–3 μm and 50–100 nm, respectively. The diameters of UPEF are 15–25 μm. The surface of UPEF shows a tightly packed fibrillar structure, as shown in the continuous large axial corrugations in Fig. 3b. The specific morphology is attributed to that UPEF comprises a complex hierarchy of fibril diameters, ranging from nanometer, micrometer, up to millimeter scales that

form under high draw ratios during processing [58]. Figure 3c shows the image of a UPEF that was tightly wrapped by PU, indicating a good adhesion between PU and UPEF. Figure 3d–e shows the cross-sections of the UPEF/BN/PU composite. It can be found that UPEF distributed homogeneously in BN/PU matrix. In this composite, the UPEF works as continuously filler while BN/PU works as matrix, which is illustrated by the schematic representation in Fig. 3f. It can be seen that when UPEF fibers were pulled out from the matrix, many holes and a network formed by BN/PU matrix can be seen on the cross-section of the composite, indicating that BN/PU uniformly wrapped the UPEF in the composite. This structure ensured that the BN/PU can transmit force to UPEF when UPEF/BN/PU composite bears the load, thereby improving the overall mechanical properties of the composites.

In order to investigate the structure of the composite, especially the structure of UPEF, WAXD and SAXS measurements were conducted on the composite. Figure 4a and b presents the 2D WAXD and SAXS scattering patterns of UPEF/BN/PU composites. The WAXD diffraction shows diffraction spots; meanwhile, an intense streak signal on SAXS is observed, indicating that the crystal is highly oriented along the axial direction of fiber. The azimuthal
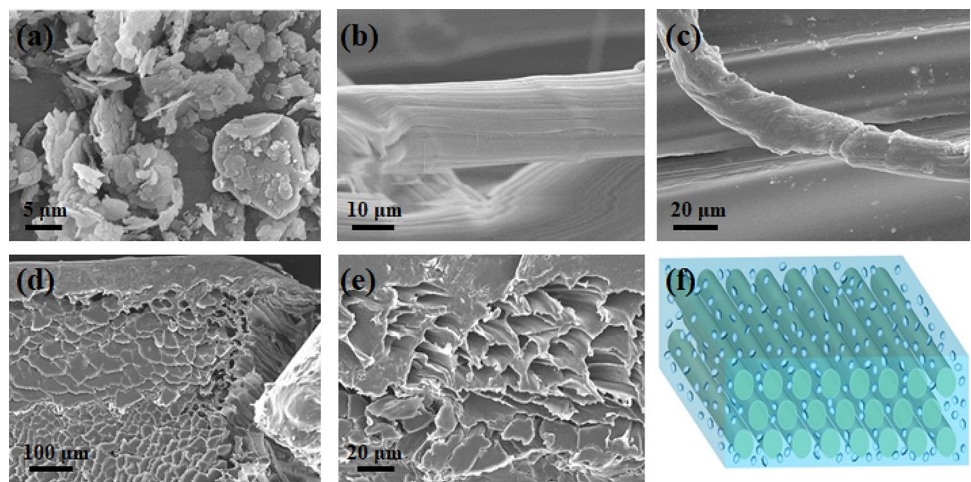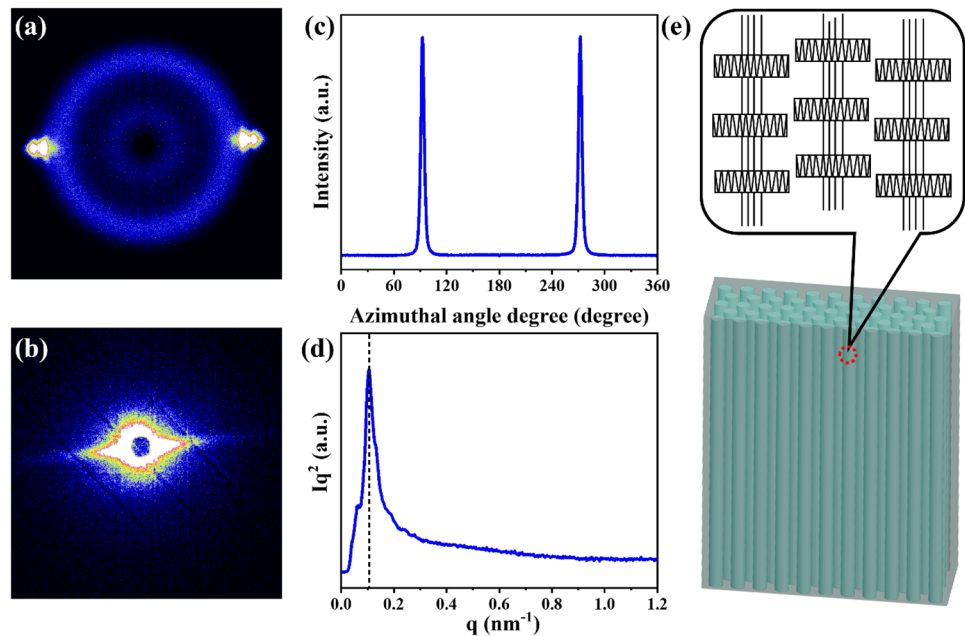
Fig. 4 **a**–**b** 2D WAXD patterns and SAXS patterns. **c** 1D WAXD azimuth integral curves, **d** 1D SAXS curves, and **e** the schematics representation of the structure of the composite


angle distribution of (002) plane is presented in Fig. 4c. It can be seen that the azimuthal angle distribution shows a sharp peak at 90° and 270°, indicating that the crystal is highly oriented along the axis direction of the fiber. The 2D SAXS diffraction patterns were integrated to obtain 1D SAXS curves, as shown in Fig. 4d. According to Bragg's law, the long period (L) can be calculated with the following equation [59]:

$$L = {^2\pi}/{q_{max}} \tag{1}$$

where q_{max} is the peak position of the corresponding 1D SAXS curves in Fig. 4d. The calculated L of polyethylene crystal in UPEF is 60.9 nm. The large L is attributed to the shish crystal, which may endow the fiber with high mechanical performance. The structure of the composite is schematically represented in Fig. 4e.

The content of BN in UPEF/BN/PU composite is an important factor that influences the neutron shielding performance. TGA measurement was conducted to determine the weight fraction of BN in the composite. As shown in Fig. 5a, for UPEF and PU, the weight decreased rapidly in the temperature range of approximately 350–500 °C, 300–450 °C, and 500–550 °C, which are corresponding to the thermal decomposition of the UPEF, soft segment of PU, and hard segment PU, respectively. Finally, UPEF and PU were completely decomposed in the test temperature range. For UPEF/BN/PU, the weight also decreases rapidly during heating due to the thermal decomposition of UPEF and PU; however, the residual weight of UPEF/ BN/PU is higher than 0% at the end heating; the residual mass is attributed to BN. The residual mass of UPEF, PU, and UPEF/BN/PU-x composites is summarized in Fig. 5b. The weight fractions of BN in UPEF/BN/PU-5, UPEF/BN/

Fig. 5 **a** TGA curves of PU, UPEF, and UPEF/BN/PU composite with various fraction of BN. **b** The weight fraction of BN content in the UPEF/BN/PU composite
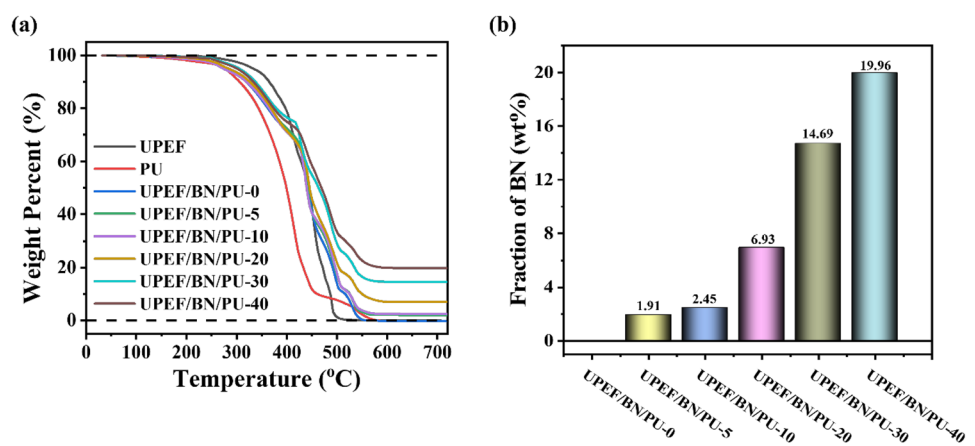
PU-10, UPEF/BN/PU-20, UPEF/BN/PU-30, and UPEF/BN/PU-40 are 1.91%, 2.45%, 6.93%, 14.69%, 19.96%, respectively. It should also be noted that with the increase of BN fraction, the decomposition temperature of the UPEF/BN/PU composites gradually increases. This may be due to that physical and chemical crosslinking points formed between BN and PU, resulting in stronger intermolecular forces in the BN–PU system [60].

3.3 The neutron shielding and mechanical properties of UPEF/BN/PU composite

As illustrated in Fig. 6a, the neutron transmission factor, I/I_0, is used to evaluate the neutron shielding capability of the UPEF/BN/PU composite with different contents of BN, where I and I_0 are the numbers of transmitted neutron fluxes with and without the shielding composite, respectively. According to the Beer–Lambert law, the attenuation of neutrons through the materials can be obtained based on the following equation [19, 38, 61]:

$$I/I_0 = \exp(-\mu \chi) \tag{2}$$

where χ is the thickness of the UPEF/BN/PU composite and μ is the linear attenuation coefficient. The mass attenuation coefficient (μ/ρ) was obtained using the following equation:

$$\mu/\rho = \frac{1}{\rho \chi} \ln(I_0/I) \tag{3}$$

where ρ is the density of the sample.

As shown in Fig. 6b, the intensity of neutron radiation can be attenuated by about 25%, 63%, and 85%, when passing UPEF/BN/PU-0 with thicknesses of 0.8, 1.6, and 3.2 mm, respectively. As no BN was added in the composite, the neutron was mainly prevented by UPEF with high hydrogen content. The result demonstrated the theoretical prediction that high content of hydrogen can shield the neutrons effectively. When the fraction of BN increased to 7 wt%, the neutron shielding performance of UPEF/BN/PU is remarkably improved, indicated by the decreasing I/I_0 value, which is attributed that boron can absorb neutron through nuclear reaction between neutrons and the nucleus of boron element in BN. The neutrons are moderated by hydrogen and absorbed by boron successively. When the fraction of BN is higher than 7 wt%, I/I_0 decreased gradually when further increasing the content of BN. The result showed that it is not realizable to improve the neutron shielding efficiency by ceaselessly adding BN fillers. Generally speaking, increased content of fillers may result in mechanical degradation of the composites; thus, the mass fraction of 7% is an optimal proportion in fabrication neutron shielding composites. In addition, the thickness of the UPEF/BN/PU composite had a significant impact on the neutron shielding performance. When the BN content is below 7 wt%, I/I_0 for UPEF/BN/PU with thickness of 1.6 mm is approximately 25–30% lower than that of UPEF/BN/PU with thickness of 0.8 mm. With the increase of BN content, the difference in the I/I_0 value between the UPEF/BN/PU composites with different thickness decreased. Figure 6c shows that μ and μ/ρ for UPEF/BN/PU composites increase as the BN content increases.

Fig. 6 **a** Schematic illustration of the setup used for neutron radiation shielding measurements. **b** Neutron transmission factor (I/I_0) versus BN content for UPEF/BN/PU composites with thickness of 0.8 mm, 1.6 mm, and 3.2 mm; **c** linear attenuation coefficient (μ), and mass attenuation coefficient (μ/ρ) versus BN content for UPEF/BN/PU composites of 1.6 mm. Note that the fraction of BN content in the x-axis is measured by TGA
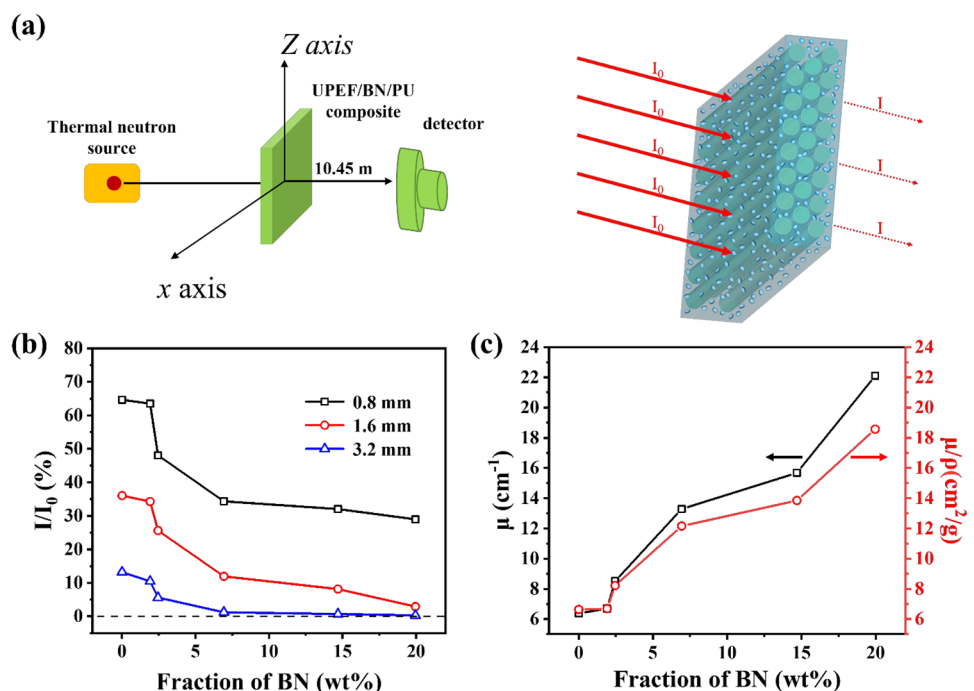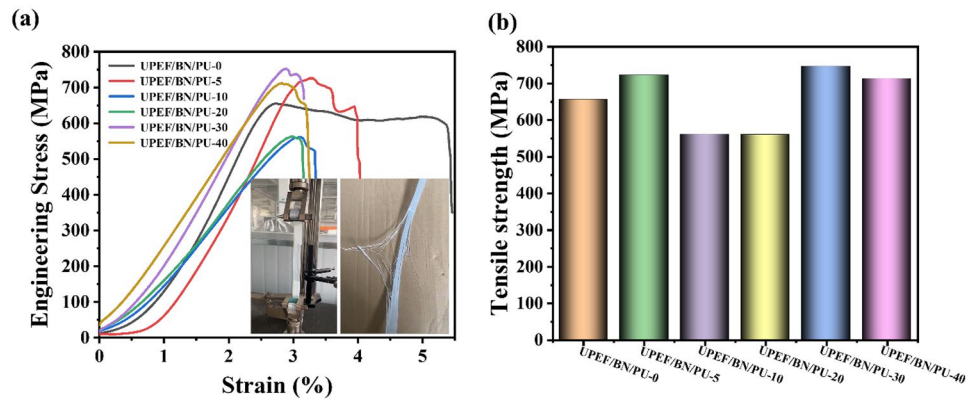
Fig. 7 **a** Engineering stress–strain curves and **b** summarized tensile strength of UPEF/BN/PU composites

The mechanical strength of the composites is measured with special clamps to avoid the slip during deformation. The engineering stress–strain curves of the UPEF/BN/PU composites in Fig. 7; the breakage of the composite is a gradually process, as the UPEF in the composite may not break together; thus, the engineering stress–strain shows a step-down decline trend when breaking. The images of the composite during deformation and after break are shown in the inset. As shown in Fig. 7b, the composites exhibit a tensile strength in the range of 550–750 MPa. It can also be found that BN content in the sample had little adverse effect on the tensile strength. This is because the strength of the composites mainly depends on the strength of UPEF. The high orientation degree of polyethylene in UPEF endows the fiber with extremely high mechanical performance. The BN/PU acts as matrix that transfer force among UPEF. The result demonstrated that the addition of BN has no obvious negative effects on the strength of the composite as the m-BN has a good interfacial bonding strength with PU.

4 Conclusion

In the present work, UPEF/BN/PU composites were fabricated by spraying BN/PU dispersion on the UPEF and subsequent hot-pressing method. The fabricated UPEF/BN/PU composites exhibit effective neutron shielding performance. For the composite with BN content of 20 wt% and thickness of 3.2 mm, the I/I_0 value was 0.28%, which means that approximately 99.72% of the neutrons were shielded. Meanwhile, the UPEF/BN/PU composites exhibit excellent mechanical properties; the tensile strength is in a range of 550–750 MPa. This ensures that the UPEF/BN/PU composites can be applied in areas with certain mechanical performance requirements. The UPEF/BN/PU composites have great potential application in aerospace, healthcare, and nuclear reactors area as efficient radiation shielding materials.

Declarations

Competing interest The authors declare no competing interests.

References

1. Chen HB, Ao YY, Liu D et al (2017) Novel neutron shielding alginate based aerogel with extremely low flammability [J]. Ind Eng Chem Res 56(30):8563–8567

2. Nagaraja N, Manjunatha HC, Seenappa L et al (2020) Gamma, X-ray and neutron shielding properties of boron polymers [J]. Indian J Pure Appl Phys 58(4):271–276

3. Huang Y, Zhang W, Liang L et al (2013) A "Sandwich" type of neutron shielding composite filled with boron carbide reinforced by carbon fiber [J]. Chem Eng J 220:143–150

4. Zhu S, Shi R, Qu M et al (2021) Simultaneously improved mechanical and electromagnetic interference shielding properties of carbon fiber fabrics/epoxy composites via interface engineering [J]. Compos Sci Technol 207:108696–108705

5. Choi G, Jeon IR, Piao H et al (2018) Highly condensed boron cage cluster anions in 2D carrier and its enhanced antitumor efficiency for boron neutron capture therapy [J]. Adv Func Mater 28(27):1704470–1704477

6. Nambiar S, Yeow JT (2012) Polymer-composite materials for radiation protection [J]. ACS Applied Material Interfaces 4(11):5717–5726

7. Tf B, Lyman J, Tobias C (1972) Visual perception of accelerated nitrogen nuclei interacting with the human retina [J]. Nature 239(5369):209–220

8. More CV, Alsayed Z, Badawi MS et al (2021) Polymeric composite materials for radiation shielding: a review [J]. Environ Chem Lett 19:2057–2090

9. Lu T, Zhang Y, Wong M et al (2017) Detection of DNA damage by space radiation in human fibroblasts flown on the International Space Station [J]. Life Sciences in Space Research 12:24–31

10. Mahesh VP, Nair PS, Rajan TPD et al (2011) Processing of surface-treated boron carbide-reinforced aluminum matrix composites by liquid–metal stir-casting technique [J]. J Compos Mater 45(23):2371–2378

11. Singh VP, Badiger NM (2015) Shielding efficiency of lead borate and nickel borate glasses for gamma rays and neutrons [J]. Glass Phys Chem 41(3):276–283

12. Sariyer D, Kucer R (2020) Effect of different materials to concrete as neutron shielding application [J]. Acta Phys Pol, A 137(4):477–479

13. Badhwar GD, Cucinotta FA (2000) A comparison of depth dependence of dose and linear energy transfer spectra in aluminum and polyethylene [J]. Radiat Res 153(1):1–8

14. Li ZF, Xue XX, Duan PN et al (2012) Preparation and thermal/fast neutron shielding properties of novel boron containing ore composites [J]. Mater Sci Forum 743:613–622

15. Agosteo S, Mereghetti A, Sagia E et al (2014) Shielding data for hadron-therapy ion accelerators: attenuation of secondary radiation in concrete [J]. Nucl Instrum Methods Phys Res, Sect B 319:154–167

16. Calzada E, Grünauer F, Schillinger B et al (2011) Reusable shielding material for neutron-and gamma-radiation [J]. Nucl Instrum Methods Phys Res, Sect A 651(1):77–80

17. El-Khayatt AM, El-Sayed AA (2009) MERCSF-N: a program for the calculation of fast neutron removal cross sections in composite shields [J]. Ann Nucl Energy 36(6):832–836

18. Almurayshid M, Alssalim Y, Aksouh F et al (2021) Development of new lead-free composite materials as potential radiation shields [J]. Materials 14:17–27

19. Zhang X, Yang M, Zhang X et al (2017) Enhancing the neutron shielding ability of polyethylene composites with an alternating multi-layered structure [J]. Compos Sci Technol 150:16–23

20. Zhang X, Zhang X, Guo S (2019) Simple approach to developing high-efficiency neutron shielding composites [J]. Polym Eng Sci 59(s2):E348–E355

21. Herrman K, Baxter LN, Mishra K et al (2019) Mechanical characterization of polyethylene-based thermoplastic composite materials for radiation shielding [J]. Composites Communications 13:37–41

22. Guetersloh S, Zeitlin C, Heilbronn L et al (2006) Polyethylene as a radiation shielding standard in simulated cosmic-ray environments [J]. Nucl Instrum Methods Phys Res, Sect B 252(2):319–332

23. Hughes GB, Mani V, Prasad NS et al (2016) Ultra high molecular weight polyethylene (UHMWPE) fiber epoxy composite hybridized with gadolinium and boron nanoparticles for radiation shielding [J]. Planetary Defense and Space Environment Applications 9981:1–10

24. Cao X, Xue X, Jiang T et al (2010) Mechanical properties of UHMWPE/Sm_2O_3 composite shielding material [J]. J Rare Earths 28:482–484

25. Firouzi D, Ching CY, Rizvi SN et al (2019) Development of oxygen-plasma-surface-treated UHMWPE fabric coated with a mixture of SiC/polyurethane for protection against puncture and needle threats [J]. Fibers 7(5):46–59

26. Du J, Wang Z, Yu J et al (2018) Ultrahigh-strength ultrahigh molecular weight polyethylene (UHMWPE)-based fiber electrode for high performance flexible supercapacitors [J]. Adv Func Mater 28(20):1707351–1707361

27. Chih A, Ansón-Casaos A, Puértolas JA (2017) Frictional and mechanical behaviour of graphene/UHMWPE composite coatings [J]. Tribol Int 116:295–302

28. Chen S, Cao Y, Feng J (2014) Polydopamine as an efficient and robust platform to functionalize carbon fiber for high-performance polymer composites [J]. ACS Applied Material Interfaces 6(1):349–356

29. Candadai AA, Weibel JA, Marconnet AM (2019) Thermal conductivity of ultrahigh molecular weight polyethylene: from fibers to fabrics [J]. ACS Applied Polymer Materials 2(2):437–447

30. Zhong WH, Sui G, Jana S et al (2009) Cosmic radiation shielding tests for UHMWPE fiber/nano-epoxy composites [J]. Compos Sci Technol 69(13):2093–2097

31. Özdemir T, Güngör A, Reyhancan İA (2017) Flexible neutron shielding composite material of EPDM rubber with boron trioxide: mechanical, thermal investigations and neutron shielding tests [J]. Radiat Phys Chem 131:7–12

32. Kim J, Lee B-C, Uhm YR et al (2014) Enhancement of thermal neutron attenuation of nano-B_4C, -BN dispersed neutron shielding polymer nanocomposites [J]. J Nucl Mater 453(1–3):48–53

33. Han H, Sun H, Lei F et al (2021) Flexible ethylene-vinyl acetate copolymer/fluorographene composite films with excellent thermal conductive and electrical insulation properties for thermal management [J]. ES Materials & Manufacturing 15:53–64

34. Zhang X, Dong J, Pan D et al (2021) Constructing dual thermal conductive networks in electrospun polyimide membranes with highly thermally conductivity but electrical insulation properties. Adv Compos Hybrid Mater 1–11

35. Tamayo P, Thomas C, Rico J et al (2020) Review on neutron-absorbing fillers [J]. Micro and Nanostructured Composite Materials for Neutron Shielding Applications 2:25–52

36. Gao S, Zhao X, Fu Q et al (2022) Highly transmitted silver nanowires-SWCNTs conductive flexible film by nested density structure and aluminum-doped zinc oxide capping layer for flexible amorphous silicon solar cells [J]. J Mater Sci Technol 126:152–160

37. Pan D, Yang G, Abo-Dief HM et al (2022) Vertically aligned silicon carbide nanowires/boron nitride cellulose aerogel networks enhanced thermal conductivity and electromagnetic absorbing of epoxy composites [J]. Nano-Micro Letters 14(1):117–135

38. Shang Y, Yang G, Su F et al (2020) Multilayer polyethylene/hexagonal boron nitride composites showing high neutron shielding efficiency and thermal conductivity [J]. Composites Communications 19:147–153

39. Xie P, Liu Y, Feng M et al (2021) Hierarchically porous Co/C nanocomposites for ultralight high-performance microwave absorption [J]. Advanced Composites and Hybrid Materials 4(1):173–185

40. Qi G, Liu Y, Chen L et al (2021) Lightweight Fe_3C@Fe/C nanocomposites derived from wasted cornstalks with high-efficiency microwave absorption and ultrathin thickness [J]. Advanced Composites and Hybrid Materials 4(4):1226–1238

41. Wu H, Sun H, Han F et al (2021) Negative permittivity behavior in flexible carbon nanofibers- polydimethylsiloxane films [J]. Engineered Science 17:113–120

42. Wu H, Zhong Y, Tang Y et al (2021) Precise regulation of weakly negative permittivity in $CaCu_3Ti_4O_{12}$ metacomposites by synergistic effects of carbon nanotubes and grapheme [J]. Advanced Composites and Hybrid Materials 5(1):419–430

43. Xie P, Zhang Z, Wang Z et al (2019) Targeted double negative properties in silver/silica random metamaterials by precise control of microstructures [J]. Research 2019:1021368–1021378

44. Soltani Z, Beigzadeh A, Ziaie F et al (2016) Effect of particle size and percentages of Boron carbide on the thermal neutron radiation shielding properties of HDPE/B_4C composite: Experimental and simulation studies [J]. Radiat Phys Chem 127:182–187

45. Schrempp-Koops L (2013) Size effects on the efficiency of neutron shielding in nanocomposites– a full-range analysis [J]. Int J Nanosci 12(03):1350015–1350023

46. Chen F, Xiao H, Peng ZQ et al (2021) Thermally conductive glass fiber reinforced epoxy composites with intrinsic self-healing capability [J]. Advanced Composites and Hybrid Materials 4(4):1048–1058

47. Yan H, Dai X, Ruan K et al (2021) Flexible thermally conductive and electrically insulating silicone rubber composite films with BNNS@ Al_2O_3 fillers [J]. Advanced Composites and Hybrid Materials 4(1):36–50

48. Yang D, Ni Y, Kong X et al (2019) Mussel-inspired modification of boron nitride for natural rubber composites with high thermal conductivity and low dielectric constant [J]. Compos Sci Technol 177:18–25

49. Wang N, Guo S, Liao J et al (2019) Surface modification of boron nitride by bio-inspired polydopamine and different chain length polyethylenimine co-depositing [J]. Polym Adv Technol 30(11):2918–2926

50. Kim Y, Kim J (2020) Carbonization of polydopamine-coating layers on boron nitride for thermal conductivity enhancement in hybrid polyvinyl alcohol (PVA) composites [J]. Polymers (Basel) 12(6):1410–1420

51. Kim K, Kim M, Kim J (2014) Enhancement of the thermal and mechanical properties of a surface-modified boron nitride-polyurethane composite [J]. Polym Adv Technol 25(8):791–798

52. Chaurasia A, Parashar A, Mulik RS (2020) Effect of hexagonal boron nitride nanoplatelet on crystal nucleation, mechanical behavior, and thermal stability of high-density polyethylene-based nanocomposites [J]. Macromol Mater Eng 305(7):2000248–2000259

53. Clausi M, Zahid M, Shayganpour A et al (2022) Polyimide foam composites with nano-boron nitride (BN) and silicon carbide (SiC) for latent heat storage. Adv Compos Hybrid Mater 1–15

54. Liu C, Fang Q, Wang D et al (2019) Carbon and boron nitride nanotubes: structure, property and fabrication [J]. ES Materials & Manufacturing 3(2):2–15

55. Yang H, Ng B C, Yu HC et al (2021) Mechanical properties study on sandwich hybrid metal/(carbon, glass) fiber reinforcement plastic composite sheet. Adv Compos Hybrid Mater 1–8

56. Peng M, Sun L, Chen L et al (2016) A new small-angle neutron scattering spectrometer at China Mianyang research reactor [J]. Nucl Instrum Methods Phys Res, Sect A 810:63–67

57. Chen L, Sun L, Wang Y et al (2016) Small-angle neutron scattering spectrometer Suanni equipped with ultra-thin biconcave focusing lenses [J]. J Appl Crystallogr 49(4):1388–1393

58. Stockdale TA, Cole DP, Staniszewski JM et al (2020) Hierarchical mechanisms of lateral interactions in high-performance fibers [J]. ACS Applied Material Interfaces 12(19):22256–22267

59. Lu Y, Lyu D, Tang Y et al (2020) Effect of α_c-relaxation on the large strain cavitation in polyethylene [J]. Polymer 210:123049–123061

60. Kim K, Kim M, Hwang Y et al (2014) Chemically modified boron nitride-epoxy terminated dimethylsiloxane composite for improving the thermal conductivity [J]. Ceram Int 40(1):2047–2056

61. El-Khayatt AM (2011) NXcom – a program for calculating attenuation coefficients of fast neutrons and gamma-rays [J]. Ann Nucl Energy 38(1):128–132